Electronic Supplementary Material (ESI) for Physical Chemistry Chemical Physics.
This journal is © the Owner Societies 2018

Electronic Supplementary Information

Photon catalysis of deuterium iodide photodissociation

Kallie I. Hilsabeck [†a], Jana L. Meiser [†a], Mahima Sneha [†a],
N. Balakrishnan[b], Richard N. Zare[a*]

[a] Department of Chemistry, Stanford University,
Stanford, CA, 94305, USA
[b] Department of Chemistry and Biochemistry, University of Nevada, Las Vegas,
Las Vegas, NV, 89154, USA

[†] These authors contributed equally to this research.

All correspondence should be addressed to rnz@stanford.edu.

Supplementary Information Table of Contents

Description of Background Subtraction Method

Laser powers were chosen to minimize background associated with nonresonant, multiphoton dissociation and ionization processes – for example, absorption of IR + UV photons to produce D^+ ions. It should be noted that no signal was observed from absorption of the IR laser alone, as the laser's focal intensity was insufficient to cause multiphoton excitation or ionization of the molecules ion the interaction volume. Any remaining background was subtracted using the two-shot method, schematically illustrated in Figure S1.

In the first shot, raw signal was collected, consisting of both true signal and background events. For Doppler-free experiments, in the first shot, all three lasers (UV_1, UV_2, and IR) were overlapped in time (Figure S1a). For pump-probe experiments, the IR pulse was overlapped with the pump pulse, and the probe pulse was delayed by 3 ns (Figure S1b). The delay was used to reduce the multiphoton ionization process caused by the overlap of the IR and probe lasers, which was found to eliminate a major source of background. The specific time delay was optimized to 3 ns to both minimize multiphoton processes while also maximizing the ionization yield. This is important in our experiments because the D atoms are formed at a very high lab-frame speed and could otherwise escape the focal volume before ionization.

In the second shot, background signal was collected: the IR pulse was overlapped with only one of the UV lasers in time, UV_1. The remaining UV laser, UV_2, was offset by 50 ns so that no true signal from the pump-probe is generated in this shot. By subtracting the background signal from the raw signal, we accounted for nonresonant, multiphoton processes arising from overlap of the IR laser with UV_1. An illustrative representation of the speed distributions measured from the raw signal, background signal, and final signal are presented in Figure S1c. The advantage of the two-shot method is that it allows us to collect the background in the same scan as that of signal, thereby eliminating any discrepancies caused by laser power fluctuations between different sets of experiments.

For this two-shot method, the UV laser that was observed to produce the most background signal with the IR laser was assigned as UV_1. For most experiments, the laser power of UV_2 could be maintained at a power that contributed negligibly to nonresonant processes. However, when background from UV_2 + IR was observed, an additional background scan was performed to account for it. The background scan was collected under the same conditions as the signal scan, but with the UV_1 laser switched off. The speed distributions presented in this work represent the final signal: raw signal – background signal 1 (UV_1 + IR) – background signal 2 (UV_2 + IR).

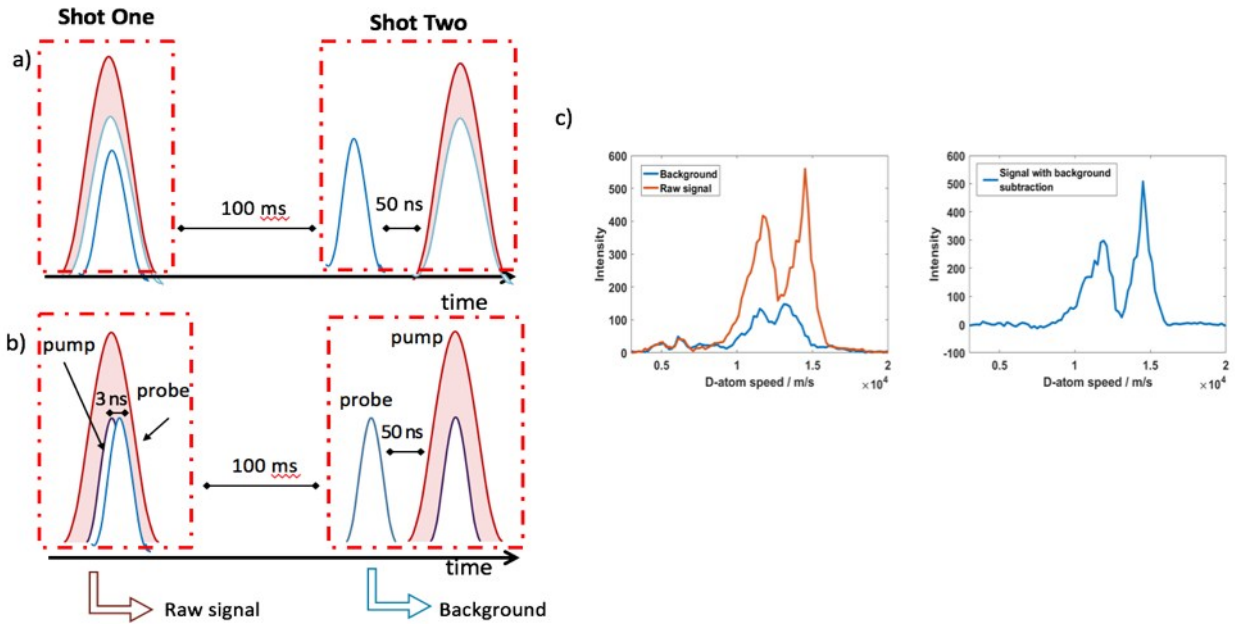

Fig. S1 Schematic diagram of the two-shot background subtraction method described in the text for the a) Doppler-free and b) pump-probe cases. The red curve represents the IR pulse, and the blue and purple curves represent the two UV laser pulses. c) Representative speed distributions for raw signal (left, orange), background signal (left, blue), and final signal = raw signal – background signal 1 (right, blue).

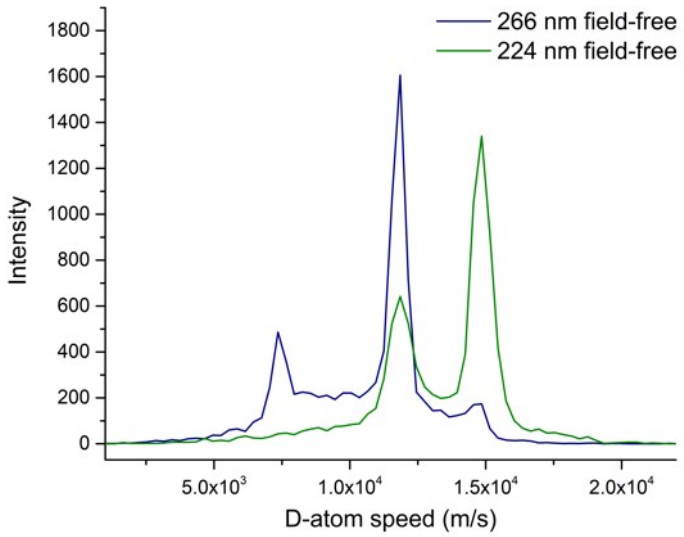

Fig. S2 D-atom speed distributions collected using the Doppler-free technique at excitation wavelengths of 266 nm (blue line) and 224 nm (green line) under field-free conditions. The slow channel produced at 224 nm clearly overlaps with the fast channel of 266 nm at our resolution of about 250 m/s, making it impossible to separate the two contributions to the total photodissociation. The speeds produced by 266-nm dissociation are very close to the speeds produced at 265 nm, and are used as justification for choosing the pump-probe technique.

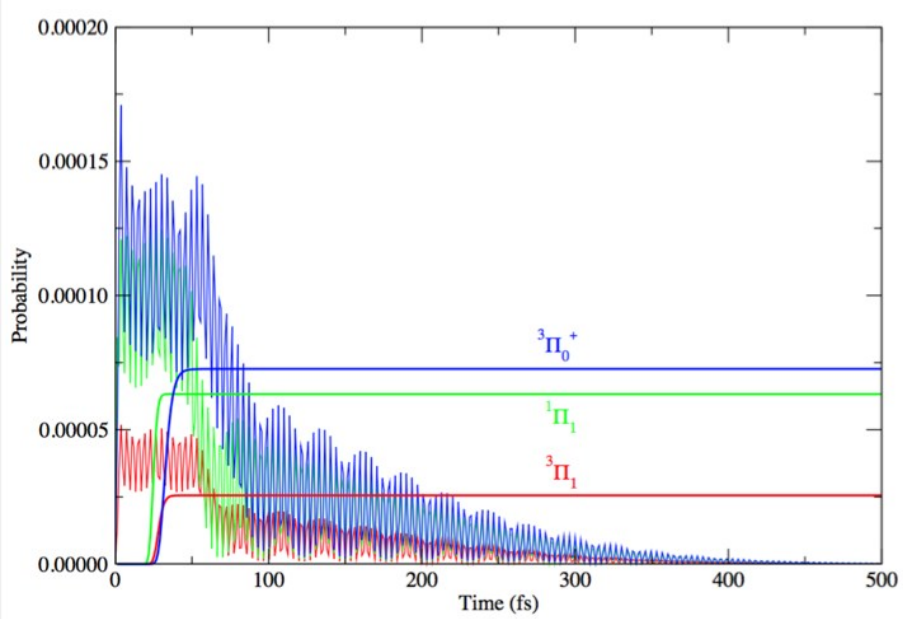

Fig. S3 Probability of excitation and dissociation on the three excited electronic states of DI, as a function of time. Both time-dependence of the probabilities and the time-integrated probabilities are shown.

Supporting Calculations for Polarizabilities of the Excited States of HI

Results of preliminary calculations of polarizabilities of HI were performed using equation of motion coupled cluster singles and doubles (EOM-CCSD) with Q-Chem[1]. These values are provided in Table S1. The computed values for the ground state are in close agreement with those reported by Maroulis.[2] The basis set used is the quadruple-ζ with extra polarization and diffuse functions (def2-QZVPPD) of Weigend and Ahlrichs.[3] The 28 electron def2 effective core potential that accounts for scalar relativistic effects was used for the iodine atom. The isotropic polarizability is calculated as $\frac{1}{3}(\alpha_{xx} + \alpha_{yy} + \alpha_{zz})$ while the anisotropic polarizability is evaluated as $\sqrt{\frac{1}{2}\left((\alpha_{xx} - \alpha_{yy})^2 + (\alpha_{yy} - \alpha_{zz})^2 + (\alpha_{zz} - \alpha_{xx})^2\right)}$. The scaled values of the polarizabilities adopted in the wave packet simulations, in particular, those corresponding to shift2, are generally consistent with the values for $^3\Pi$ and $^1\Pi$ states given in Table S1. More detailed calculations including spin-orbit coupling are beyond the scope of this work.

Table S1. Dipole moment and polarizabilities of the ground state and excited $^3\Pi$ and $^1\Pi$ states of HI corresponding to a bond distance of 3.04 bohr.

State	Excitation Energy (eV)	Excitation Energy (nm)	Dipole Moment (au)	Isotropic Polarizability (au)	Anisotropic Polarizability (au)
$^1\Sigma_{0+}$	0.00	0.00	0.182194	35.017	2.791
$^3\Pi$	5.1981	238.52	0.277526	54.034	53.911
$^1\Pi$	5.7064	217.27	0.232328	66.225	77.184

(1) Shao, Y.; Gan, Z.; Epifanovsky, E.; Gilbert, A. T. B.; Wormit, M.; Kussmann, J.; Lange, A. W.; Behn, A.; Deng, J.; Feng, X.; et al. Advances in Molecular Quantum Chemistry Contained in the Q-Chem 4 Program Package. *Mol. Phys.* **2015**, *113* (2), 184–215.

(2) Maroulis, G., Is the dipole polarizability of hydrogen iodide accurately known? *Chem. Phys. Lett*. 2**000**, 318, 181.

(3) Weigend, F.; Ahlrichs, R. Balanced Basis Sets of Split Valence, Triple Zeta Valence and Quadruple Zeta Valence Quality for H to Rn: Design and Assessment of Accuracy. *Phys. Chem. Chem. Phys.* **2005**, *7* (18), 3297.

Table S2. D-atom slow and fast channel peak speeds measured at different excitation wavelengths, using a (2+1) REMPI detection scheme centered approximately at 243 nm.

Pump wavelength (nm)	Probe wavelength (nm)	v_fast (m/s)	v_slow (m/s)
213*	213, 283	15800	13300
216*	216, 278	15800	12800
224*	266	14800	11900
230	243	14300	11100
243*	243	13700	10500
265	243	11700	7600
266*	224	11900	7700
278*	278, 216	11300	6200

* For the measurements using the Doppler-free probing technique, the UV lasers are set at wavelengths such that together they are resonant to the 2s←1s two photon excitation of the D atom.

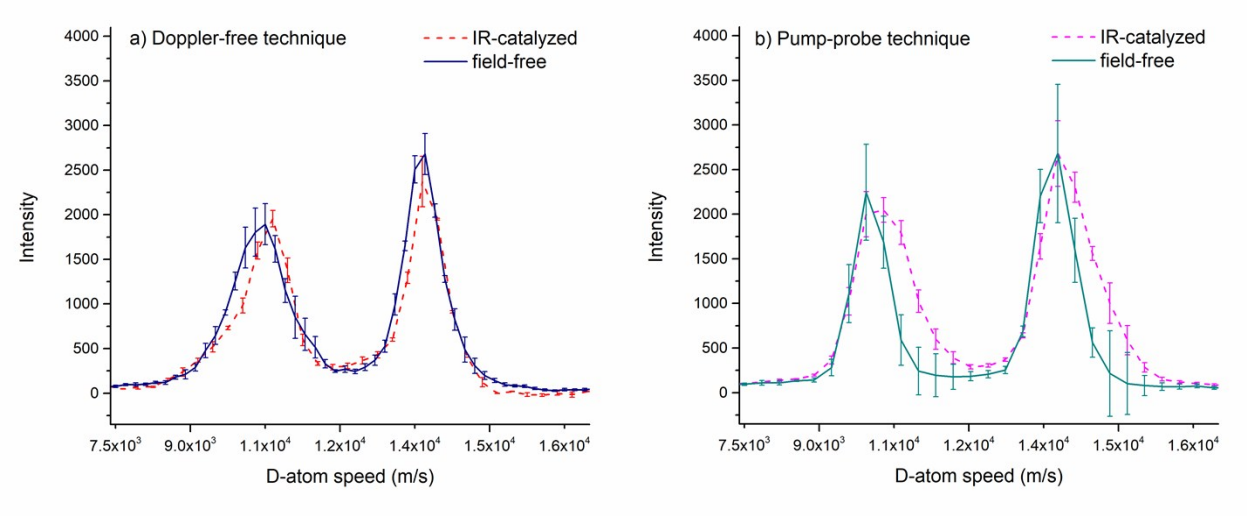

Fig. S4 D-atom speed distributions collected at an excitation wavelength of 243 nm using a) the Doppler-free technique (blue solid line – field-free, red dashed line – IR-catalyzed) and b) the pump-probe technique (turquoise solid line – field-free, pink dashed line – IR-catalyzed). The relative branching ratio change with the application of the electric field, i.e. no significant change to one standard deviation, is the same for both detection techniques, despite the apparent widening of the peaks in the presence of the IR field in b). Although the measured effect of the IR field was the same for both techniques, the Doppler-free data were chosen for presentation in the manuscript for two reasons: the absolute branching ratio under field-free conditions more closely approximated previous experimental and theoretical results, and the cleaner experimental setup gave well-defined Gaussian peaks in the speed distribution.

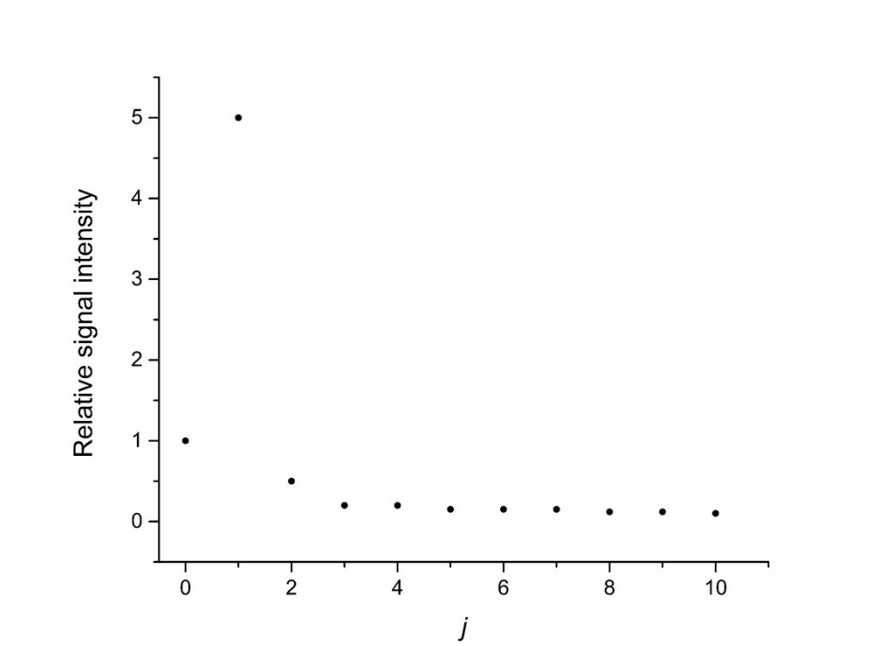

Fig. S5 Estimate of DI rotational distribution of molecules in lower *j* levels in the molecular beam. There is detectable population up to *j* = 10, measured by DI (2+1) REMPI.